Forward Transit Delay in $In_{0.53}Ga_{0.47}As$ Heterojunction Bipolar Transistors with Nonequilibrium Electron Transport

Joy Laskar, *Member, IEEE*, Richard N. Nottenburg, *Member, IEEE*, J. A. Baquedano, Anthony F. J. Levi, and James Kolodzey, *Senior Member, IEEE*

***Abstract*—The microwave performance of high speed $InP/In_{0.53}Ga_{0.47}As$ Heterojunction bipolar transistors is measured in the temperature range 55 K $\leq T \leq$ 340 K. The extrinsic unity currents gain cut-off frequency is f_T = 130 GHz at temperature T = 340 K increasing to f_T = 300 GHz at T = 55 K. The intrinsic emitter-collector forward delay decreases with decreasing temperature from τ_F = 0.5 ps at T = 340 K to a saturated value of τ_F = 0.28 ps for temperatures $T \leq$ 150 K. Such behavior may only be explained by the presence of nonequilibrium electron transport in the base and collector of the device.**

I. Introduction

THE existence of extreme nonequilibrium electron transport in abrupt $Al_{0.48}In_{0.52}As/In_{0.53}Ga_{0.47}As$ and $InP/In_{0.53}Ga_{0.47}As$ heterojunction bipolar transistors (HBTs) has been previously demonstrated by studying static transistor characteristics [1]–[4]. For example, in recent work it has been empirically established that extreme nonequilibrium electron transport in the base of an abrupt $Al_{0.48}In_{0.52}As/In_{0.53}Ga_{0.47}As$ HBT causes current gain β to vary approximately as $1/x_B$, where x_B is the base thickness [1]. This result contrasts with the $1/x_B^2$ scaling of base recombination limited current gain in conventional bipolar transistors with diffusive charge transport in the base. In addition, avalanche multiplication in the collector of abrupt $Al_{0.48}In_{0.52}As/In_{0.35}Ga_{0.47}As$ HBT's is found to depend on base width [3]. Apart from confirming the existence of nonequilibrium base transport this illustrates the fact that base and collector transport are dependent quantities. In this situation the intrinsic collector delay τ_C depends on the base transit delay τ_B and, therefore, the relevant single physical quantity to be measured is the intrinsic (i.e., without parasitic charging times) emitter-collector delay τ_F. Of course, τ_F is itself controlled by electron dynamics in the base and collector, so knowledge about electron scattering mechanisms leads to a more complete understanding of device operation.

We have performed a comprehensive study of the high frequency current gain h_{21} in the temperature range 55 K $\leq T \leq$ 340 K. Detailed device modeling was used to extract τ_F from the measured data. These results show that intrinsic emitter-collector forward delay decreases from a value of τ_F = 0.5 ps at a temperature T = 340 K and saturates at a value of $\tau_F \sim$ 0.28 ps for, temperature T = 150 K and below. This marked decrease in measured forward delay with decreasing temperature arises from the temperature dependence of electron scattering in the device. The extrinsic current gain cutoff frequency, f_T, of these devices at a temperature of T = 55 K is greater than 300 GHz. Such a high value of f_T may only be explained by the existence of extreme nonequilibrium electron transport in the base and collector. An average electron velocity of around 4.5×10^7 cm s^{-1} through the base and 8×10^{17} cm s^{-1} through the collector excludes the possibility that electron motion in these devices can be described by conventional or drift-diffusive transport.

II. Device Design

Mesa transistors with an emitter area $A_E = 3.5 \times 3.5$ μm^2 were fabricated from crystals with the layer structure shown in Table I. The ideality of the emitter-base junction is n = 1.3 and that of the collector is n = 1.0. This fact is reflected in the static transfer characteristics of the device. As may be seen in Fig. 1, the slope of the base and collector currents with increasing V_{BE} are the same. Another point worth mentioning is that, because of the high base doping $p = 1 \times 10^{20}$ cm^{-3}, the base sheet resistance is low, R_B = 400 Ω square^{-1}. This low sheet resistance is important as it allows some design flexibility. In particular, a wider emitter finger can be used without raising the parasitic resistance. This relaxes the scaling limitations and results in a small emitter area to collector area ratio of 1/1.3.

In Fig. 2 we show a band diagram for a npn InP/InGaAs HBT with a conduction band discontinuity

Manuscript received July 22, 1992; revised June 10, 1993. J. A. Baquedano was supported in part by AT&T Microelectronica España through the IPSB program. J. Laskar was supported by grants from Hewlett-Packard and Cascade Microtech, Inc. The review of this paper was arranged by Associate Editor N. Moll.

J. Laskar is with the Department of Electrical Engineering, University of Hawaii, Honolulu, HI 96822.

R. N. Nottenburg is with Department of Electrical Engineering and Electrophysics, University of Southern California, Los Angeles, CA 90089.

J. A. Baquedano is with AT&T Microelectronica España, 28760 Tres Cantos, Mardrid, Spain.

A. F. J. Levi is with the Department of Electrical Engineering and Electrophysics, University of Southern California, Los Angeles, CA 90089.

J. Kolodezy is with the Department of Electrical Engineering,University of Delaware, Newark, DE 19716.

IEEE Log Number 9211730.

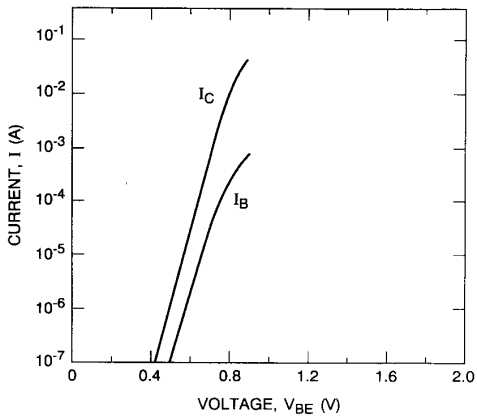

Fig. 1. Static transfer characteristics of an abrupt $InP/In_{0.53}Ga_{0.47}As$ n-p-n HBT. Device layer structure is the same as shown in Table I. Ideality factor for the emitter-base junction is $n = 1.3$ and $n = 1.0$ for the base-collector junction. $A_E = 2.7 \times 10^{-7}$ cm^2 and measurements were performed at temperature $T = 300$ K.

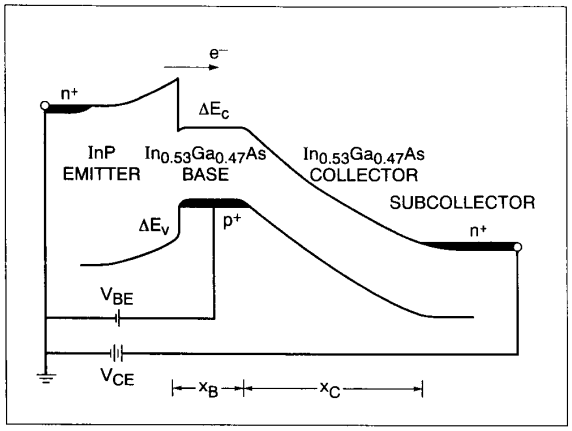

Fig. 2. Schematic band diagram of an abrupt $InP/In_{0.53}Ga_{0.47}As$ n-p-n HBT under base-emitter bias, V_{BE}, and collector emitter bias, V_{CE}. Conduction band off-set ΔE_C and valence band off-set ΔE_V are indicated.

TABLE I
InP/InGaAs HBT Layer Structure

Layer	Material	Doping (cm^{-3})	Thickness (Å)
Cap	n-InGaAs	7×10^{19}	2000
Emitter	n-InP	1×10^{18}	3000
Base	p-InGaAs	1×10^{20}	500
Collector	n-InGaAs	2×10^{16}	3000
Subcollector	n-InGaAs	5×10^{19}	2500
Substrate	S.I. InP		

$\Delta E_c = 0.26$ eV and a valence band discontinuity $\Delta E_V = 0.34$ eV [5]. The static (dc) common emitter current gain $\beta \sim 50$ is limited by back injection of holes from the heavily doped $p = 1 \times 10^{20}$ cm^{-3} base into the emitter [5]. The abrupt heterojunction design allows both high speed performance and adequate current gain.

The device operates by injecting electrons from the emitter into the base with an excess kinetic energy of $E \sim 0.26$ eV and initial velocity of around 1×10^8 cm s^{-1}. While traversing the base of thickness x_B each electron has a probability of inelastically or elastically scattering by angle Θ and changing kinetic energy by $\hbar\omega$. After traversing the base a nonequilibrium distribution of electrons encounters and accelerates in the electric field of the collector. While in the collector electrons may experience various scattering processes including polar-optic, intervalley, and electron–electron collisions. All of these events contribute to the collector delay.

III. High-Frequency Results

Transistor scattering parameters were measured in the frequency range 0.5 to 26.5 GHz using a HP8510B network analyzer and Cascade Microtech high frequency probes. These measurements were performed over the temperature range 55 K $\leq T \leq$ 340 K by integrating the high frequency probes into a vacuum chamber where effects due to moisture and changing temperature gradients across the microwave hardware were eliminated [6]. An accurate calibration procedure is achieved by measuring short-open-load through calibration standards on a standard substrate with known impedance co-located with the test device. Calibration integrity is verified at each temperature by measuring the reflection coefficient from an open circuit stub.

The surface temperature of the wafer stage is monitored with a thermocouple attached to the sample substrate. The actual device temperature is determined by measuring the current-voltage characteristics of the collector-base diode which has an ideality factor of $n = 1.0$. By controlling the flow rate, pressure and temperature of nitrogen gas the sample temperature may be varied from $T = 150$ to 340 K. For lower temperatures helium gas is used as the coolant.

The forward current gain h_{21} derived from S-parameters follows a -6 dB/octave roll-off and extrapolates to the short circuit unity gain cutoff frequency, f_T, at $h_{21} = 0$. In Fig. 3 we show typical dependence of h_{21} with frequency at a temperature $T = 55$ K, which extrapolates to f_T greater than 300 GHz. The total emitter—collector delay time, τ_{EC} is related to f_T via

$$\frac{1}{2\pi f_T} = \tau_{EC} = \tau_E + \tau_{CC} + \tau_F \qquad (1)$$

where τ_E is the emitter charging time, τ_{CC} is the collector charging time and τ_F is the intrinsic forward delay. Contributing to τ_F is the base transit delay, τ_B and the collector space charge delay τ_C. The intrinsic forward delay may be accurately determined by equivalent circuit modeling. After the on wafer calibration procedure, S-parameter data at each temperature is recorded. The S-parameter data is then used to construct the small-signal equivalent circuit shown in Fig. 4(a) which represents the physical operation of the device. The pad capacitance C_{P1} and C_{P2} are determined from the measured Y-parameters of an open device as described in [7]. The emitter, base, and collec-

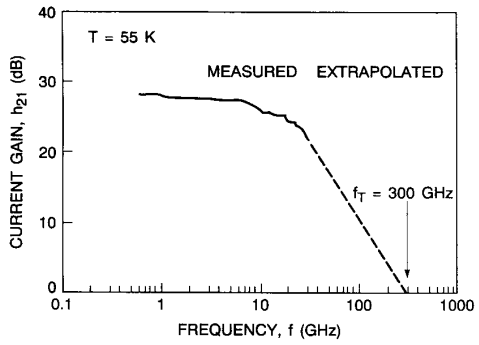

Fig. 3. h_{21} as a function of frequency for an abrupt $InP/In_{0.53}Ga_{0.47}As$ n-p-n HBT at temperature $T = 55$ K. The extrapolated cut-off frequency is $f_T = 300$ GHz. $V_{CE} = 1.2$ V, $I_C = 15$ mA, and $A_E = 1.2 \times 10^{-7}$ cm^2.

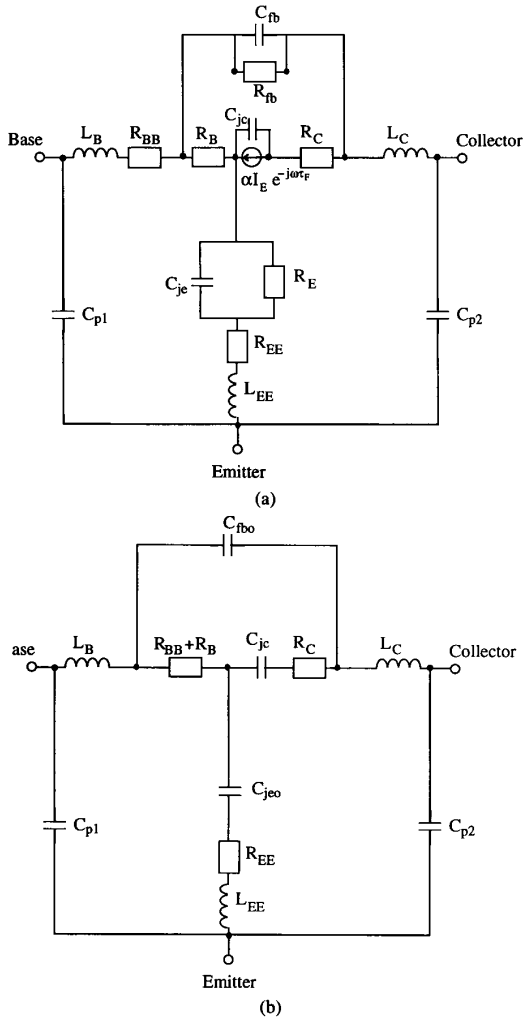

Fig. 4. (a) Equivalent circuit including parasitics. (b) Simplified equivalent circuit.

tor inductances are calculated from the Z-parameters under forward bias conditions for the emitter-base and base-collector junctions, analogous to the technique outlined

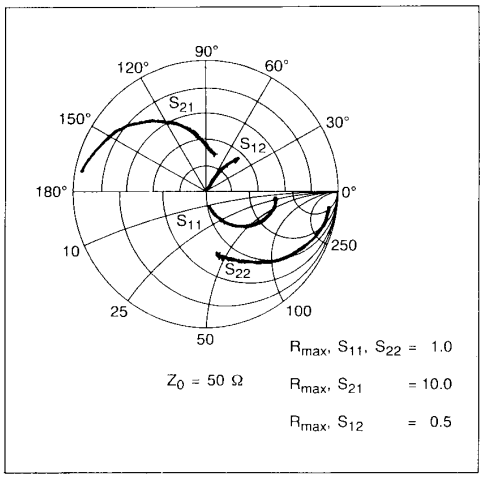

Fig. 5. S-parameters for an abrupt $InP/In_{0.53}Ga_{0.47}As$ n-p-n HBT at temperature $T = 55$ K. $V_{CE} = 1.1$ V, $I_C = 13$ mA, and $A_E = 1.2 \times 10^{-7}$ cm^2. Both the measured and model data (fit to the small-signal equivalent circuit in Fig. 4(a)) fall within the solid bold lines of the figure. R_{max} represents the radius of the Smith Charts used for each s-parameter.

for field-effect transistors in [8] and using the equations derived for the "T" type circuit model [9]. The values of C_{P1}, C_{P2}, L_E, L_B, and L_C are verified by fitting the measured S-parameters using the simplified model of Fig. 4(b).

The value for base resistance, R_B is determined by the input impedance circle method [10]. The measured values of s_{11} form a semi-circle on the complex impedance plane. The value of R_B is the extrapolated point at which S_{11} crosses the real axis at high frequency. This is shown in Fig. 5 where $R_B \sim 49\ \Omega$ at $T = 55$ K. The data form an almost ideal semicircle indicating negligible inductance effects. These extrapolated values of R_B agree well (within 5%) with the estimated values of R_B derived from dc measurements on transmission line test patterns on the same wafer. The value of C_{je0} is calculated from the imaginary component of the measured input reflection coefficient of the device under zero bias conditions after removing the effect of pad parasitics. The input reflection coefficient is purely capacitive at low frequencies with no bias applied. With V_{CE} constant a value of C_{je} is extracted from the small-signal equivalent circuit at each V_{BC} bias point. We can fit C_{je}, to the relation

$$C_{je} = \frac{C_{je0}}{(1 - V_{be}/V_{bi})^{1/2}} \tag{2}$$

where $V_{bi} \sim 1$ V at $T = 300$ K. There is excellent agreement between the two techniques and the typical values for C_{je0} are 60 fF and 55 fF at $T = 300$ K and $T = 150$ K, respectively. One critical point to be noted here is the meaning of C_{je}. C_{je} does not include the frequency dependence of the so-called diffusion capacitance because of the dominance of nonequilibrium transport in such a structure. The only other bias dependent terms are the dynamic

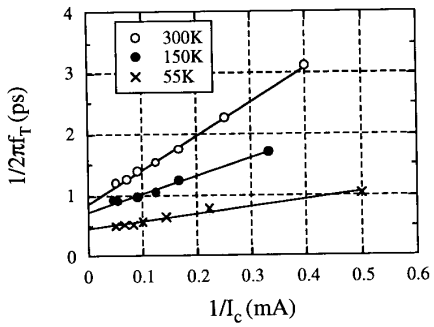

Fig. 6. Plot of $1/2\pi f_T$ vs. $1/I_C$ for an abrupt $InP/In_{0.53}Ga_{0.47}As$ n-p-n HBT at lattice temperatures of 300, 150, and 55 K with $V_{CE} = 1.1$ V. The slope of the linear fit for each temperature is proportional to the sum of the junction capacitances and the y-intercept can be used to confirm τ_F. Using this data the extracted value of τ_F has been verified to within $\pm 10\%$ as shown in Fig. 7.

TABLE II
SMALL-SIGNAL PARAMETERS FOR A n-p-n $InP/In_{0.53}Ga_{0.47}As$ HBT WITH 15 mA $\leq I_C \leq$ 20 mA, $V_{CE} =$ 1.2 V, AND $A_E = 1.2 \times 10^{-7}$ cm^{-2}

Parameter	T = 55 K	T = 150 K	T = 240 K	T = 300 K	T = 340 K
τ_F (ps)	0.27	0.28	0.38	0.45	0.50
τ_{EC} (ps)	0.50	0.88	1.06	1.18	1.24
α	0.98	0.98	0.97	0.97	0.97
C_{je} (fF)	200.1	233.9	227.2	225.6	205.7
C_{jc} (fF)	9.1	13.3	13.9	14.3	12.8
C_{fb} (fF)	15.2	21.9	20.0	19.8	19.5
R_{EE} (Ω)	5.1	9.2	8.3	8.7	8.1
R_{BB} (Ω)	1.6	2.03	1.73	1.23	1.12
R_B (Ω)	48.6	53.7	58.1	61.6	65.3
R_C (Ω)	2.3	4.33	3.41	3.68	3.37
R_E (Ω)	0.29	0.47	1.14	1.32	1.61
R_{FB} (kΩ)	7.8	12.0	11.8	10.6	10.5

emitter resistance R_E and the complex common base current gate, α. The small-signal elements R_{EE}, R_{BB}, and R_C are determined from dc measurements and are relatively insensitive to bias. Two methods are used as validity checks for the accuracy of the extracted delay times: (1) the small-signal element values are used to simulate the measured S-parameters using the equivalent circuit and (2) the values of τ_F and junction capacitances are confirmed by plotting $1/2\pi f_T$ vs. $1/I_C$ as shown in Fig. 6. The small signal-elements C_{P1}, C_{P2}, L_E, L_B, L_C, R_{EE}, R_B, R_{BB}, and R_C are fixed and are bias independent. The elements α, C_{jc}, C_{je}, and R_E are bias dependent and are computed at each bias point. The small signal element extraction may also be constrained by (1) as described in [11]. Representative values of the small-signal circuit elements are shown in Table II, with less than 10% relative error between the measured and modeled s-parameters.

The data plotted in Fig. 6 confirm the extracted values of τ_F (y-intercept) and the slope is proportional to the sum of C_{je}, C_{jc}, and C_{fb}. We estimate that the values of τ_F and C_{je} are accurate to within $\pm$ 10%, which is the relative error between the data in Fig. 6 and values from small-signal circuit simulations.

IV. DISCUSSION

In Fig. 7 we show as a function of temperature, T, the values of τ_F extrapolated from the measured S-parameter data. The small signal data is that for an abrupt *n-p-n* $InP/In_{0.53}Ga_{0.47}As$ HBT with emitter area $A_E = 1.2 \times 10^{-7}$ cm^2 under bias $V_{CE} = 1.2$ V and $I_C = 20$ mA. At a temperature $T = 340$ K the forward delay is $\tau_F = 0.50 \pm 0.05$ ps. With decreasing temperature τ_F becomes smaller saturating at a value $\tau_F \sim 0.28 \pm 0.03$ ps for $T \leq 150$ K. As seen from Table II, the dominant temperature dependent elements, as determined by their effect on the delay time, are τ_F, R_E, and R_B. R_E is proportional to the temperature and R_B is controlled by carrier mobility in the heavily doped base.

The observed temperature dependence of intrinsic forward delay, τ_F, is due to variation in electron scattering with temperature and carrier density. This may be illustrated by considering the inelastic scattering rate, $1/\tau_{in}$, for a central Γ-valley conduction band electron of initial kinetic energy $E = 150$ meV. In the neutral base electrons may scatter elastically from statically screened ionized p-type impurities or inelastically, changing kinetic energy

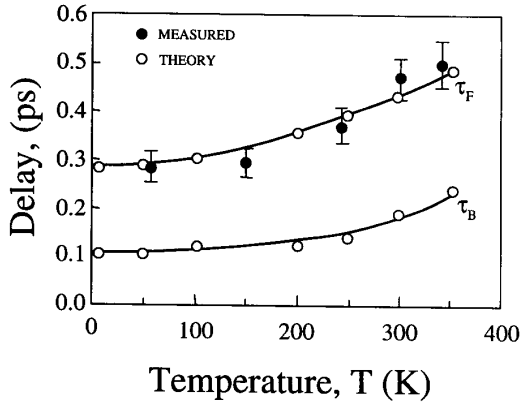

Fig. 7. Values of τ_F extracted from the measured S-parameter data and result of numerically simulating small signal delay τ_F and τ_B as a function of temperature, T. The device is an abrupt InP/$In_{0.53}Ga_{0.47}As$ n-p-n HBT. Emitter area is $A_E = 1.2 \times 10^{-7}$ cm^2, and device layer structure is the same as shown in Table I. The solid line in the figure is a least-squares fit to the simulated data points.

by $\hbar\omega$ and changing momentum by q. Electron scattering rates may be calculated within the random phase approximation using a method outlined in [12] which relates the electron self energy to the dielectric response of the semiconductor. Within this formalism, the dielectric response function is

$$\epsilon(q, \omega) = \epsilon_\infty \left\{ 1 - \frac{(\omega_{LO}^2 - \omega_{TO}^2)}{\omega(\omega + i\gamma) - \omega_{TO}^2} \right\} + \chi_e(q, \omega) \quad (3)$$

where ϵ_∞ is the high frequency dielectric constant, q is the scattered wave vector, $\hbar\omega$ is the change in energy, ω_{LO} is the longitudinal optic phonon frequency, ω_{TO} is the transverse optic phonon frequency, γ is a collision broadening term, and $\chi_e(q, \omega)$ is the electron contribution. In this case the inelastic scattering rate, $1/\tau_{in}$, is calculated using

$$\frac{1}{\tau_{in}} = \sum_{k'} \frac{-8\pi e^2}{\hbar q^2} \operatorname{Im}\left[\frac{1}{\epsilon(q, \omega)}\right] (f(E - \hbar\omega) + g(-\hbar\omega)) \quad (4)$$

where the Fermi function $f(E) = (1/\exp[(E - \mu)/k_B T] + 1)$, the Bose function $g(E) = (1/\exp[E/k_B T] - 1)$, μ is the chemical potential and k_B is Boltzmann's constant.

In Fig. 8 we show results using (3) and (4) to calculate the coupled electron-electron/optical phonon scattering rate in $In_{0.53}Ga_{0.47}As$ as a function of temperature for carrier densities $n = 0$ cm^{-3} and $n = 1 \times 10^{17}$ cm^{-3}. In both cases optical phonon scattering is important, however, for $n = 1 \times 10^{17}$ cm^{-3} the electron-electron interaction is appreciable, leading to a more rapid increase in $1/\tau_{in}$ with increasing temperature. For example, the total inelastic scattering time for a conduction band electron in the presence of $n = 1 \times 10^{17}$ cm^{-3} other electrons is less than 50 fs at $T = 300$ K compared to 124 fs for $n = 0$ cm^{-3}.

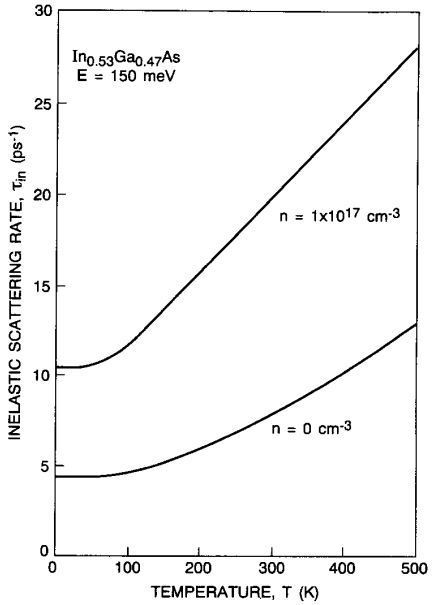

Fig. 8. Calculated total inelastic scattering rate $1/\tau_{in}$ in $In_{0.53}Ga_{0.47}As$ as a function of temperature for carrier density $n = 0$ cm^{-3} and $n = 1 \times 10^{17}$ cm^{-3}.

To obtain a more detailed understanding of the mechanisms determining the temperature dependence of τ_F, we performed Monte-Carlo simulations similar to those described in [13]–[15]. The electrons contributing to the emitter current, I_E, are initially thermally distributed in the conduction band of the wide band gap InP emitter and are then injected with excess kinetic energy $\Delta E_C = 0.26$ eV into the conduction band of the p-type $In_{0.53}Ga_{0.47}As$ base. As discussed above, the relevant scattering rates may be calculated using the appropriate dielectric response function $\epsilon(q, \omega)$ for p-type majority carriers [16], [17]. The trajectories of electrons traversing the base are calculated according to a standard semiclassical Monte-Carlo procedure and current flowing across the base-collector junction, I_{BC}, is calculated as a function of time. Having traversed the base, electrons are accelerated in the electric field of the reverse-biased collector space-charge region. Here they may suffer inelastic collisions with phonons and other electrons. Those electrons which gain enough kinetic energy may also transfer from the Γ to the relatively low velocity L- and X-valley conduction band minima. The inelastic scattering rate is larger than elastic scattering in the collector space charge region. In the base elastic and inelastic scattering rates are comparable.

Since current flow through the collector obeys Maxwell's equations, we require $\nabla \cdot (j_{el} + \partial/\partial t[D/4\pi]) = 0$ where j_{el} is current density and D is electric displacement field. The electric displacement field's contribution to current flow reduces the collector current delay by about

a factor of two compared to the electron transit time across the collector. In addition, high current density operation ($j_{e1} \sim 10^5$ cm^{-3}) and relatively low impurity concentration in the collector result in significant space-charge effects. It is, therefore, necessary to take into account band-bending by satisfying Poisson's equation in the base and collector throughout the simulation.

In Fig. 9 we show typical results of calculating response to current modulation between 12 mA and 15 mA and response to current modulation between 0 and 12 mA for a temperature $T = 50$ K. We expect I_{BC} to be delayed from I_E due to the base transit time and I_C to be delayed from I_{BC} due to collector transit time and charging. Fig. 9(a) shows the input signal I_E and the collector current output, I_C. Fig. 9(b) shows the input signal I_E, the current I_{BC}, and the electron current I_{e1}. We include I_{e1} in this figure since the electron transit time across the collector is not exactly 1/2 that of the collector current delay [18]. As may be seen, the response to large current modulation cannot be characterized by a single time constant. The factors contributing to this include the carrier density dependence of electron scattering rates.

In Fig. 7 we show results of calculating the total small signal delay, τ_F as a function of temperature, T, for conditions similar to those used in the experiments discussed above (see Table III). Also shown in the figure is the small signal base transit dely τ_B as a function of temperature. The agreement between experiment and theory is satisfactory. The physics underlying the temperature dependence of τ_F is related to the temperature dependence of $1/\tau_{in}$ illustrated in Fig. 8. At low tempertures ($T \leq 50$ K) the base transit delay $\tau_B \sim 0.11$ ps is about one third of the total forward delay $\tau_F \sim 0.30$ ps. The average electron velocity in the base is $v_B = 4.5 \times 10^7$ cm s^{-1} and in the collector it is $v_C \sim 8 \times 10^7$ cm s^{-1}. At room temperature ($T = 300$ K) $\tau_B \sim 0.19$ ps is almost half the total delay $\tau_F \sim 0.43$ ps. In this case v_B 2.6 $\times 10^7$ cm s^{-1} and $v_C \sim 6 \times 10^7$ cm^{-1}. The high average electron velocity in the base arises from nonequilibrium electron transport. A diffusive transport model cannot be justified as it would imply an unreasonably high value for minority carrier mobility of $\mu(T = 50\text{ K}) = 2.7 \times 10^4$ cm^2 V^{-1} s^{-1} and $\mu(T = 300\text{ K}) = 2.5 \times 10^3$ cm^2 V^{-1} s^{-1} for an $In_{0.53}Ga_{0.47}As$ p-type majority carrier concentration of $p = 1 \times 10^{20}$ cm^{-3}. In addition, attempts to fit the electron distribution function to an effective electron temperature, T_e, greater than the lattice temperature fail. It is therefore inappropriate to introduce an "effective diffusion constant."

The above discussion of τ_F refers to a collector-base bias voltage of $V_{CB} \sim 0.3$ V. In this situation base transport is more temperature sensitive than collector transport. The relative temperature dependent contributions of Γ-L and Γ-X scattering do not dominate. At larger reverse bias, e.g., $V_{CB} = 1$ V, more electrons scatter into the X and L valleys and the relative importance of the temperature dependence of phonon and electron–electron scattering in these valleys increases. Fig. 10 shows how this manifests itself as an enhanced temperature sensitivity of τ_F with increasing temperature and increasing V_{CB}. At values of $V_{CB} \leq 0.2$ V the temperature sensitive collector diffusive capacitance causes the experimentally determined τ_F to increase.

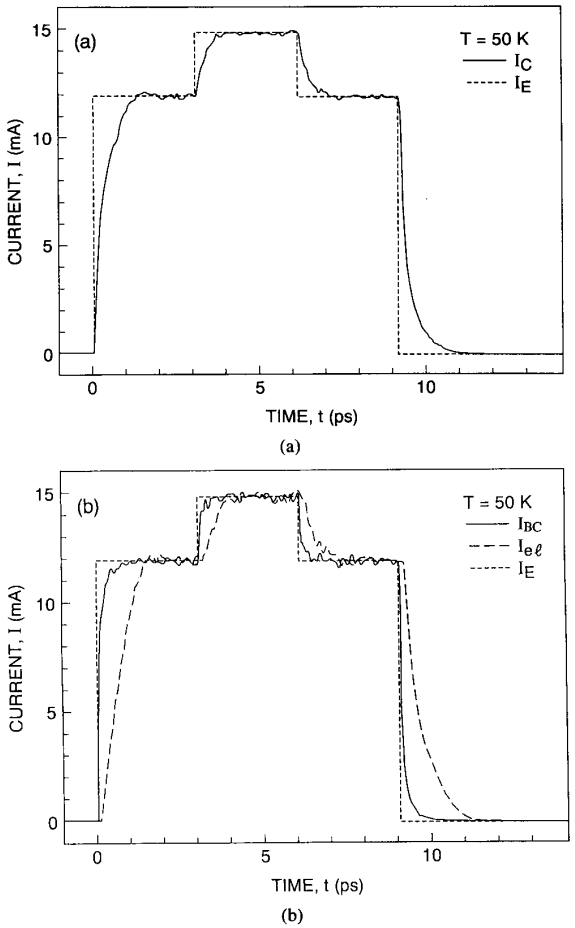

Fig. 9. Result of numerically simulating the step response of an abrupt $InP/In_{0.53}Ga_{0.47}As$ n-p-n HBT at temperature $T = 55$ K. Emitter area $A_E = 1.2 \times 10^{-7}$ cm^2 and device layer structure is the same as shown in Table I (a) shows emitter current I_E and collector current I_C as a function of time t. (b) shows emitter current I_E and base current I_{BC} flowing across the base/collector junction and electron current, I_{e1}, at the collector as a function of time, t.

TABLE III
CALCULATED SMALL-SIGNAL DELAY FOR A n-p-n $InP/In_{0.53}Ga_{0.47}As$ HBT WITH $I_C = 15$ mA, $V_{CE} = 1.2$ V, AND $A_E = 1.2 \times 10^{-7}$ cm^{-2}

Temperature (K)	τ_F (ps)	τ_B (ps)
5	0.28	0.11
50	0.30	0.11
100	0.31	0.12
200	0.36	0.12
250	0.38	0.13
300	0.43	0.19
350	0.50	0.24

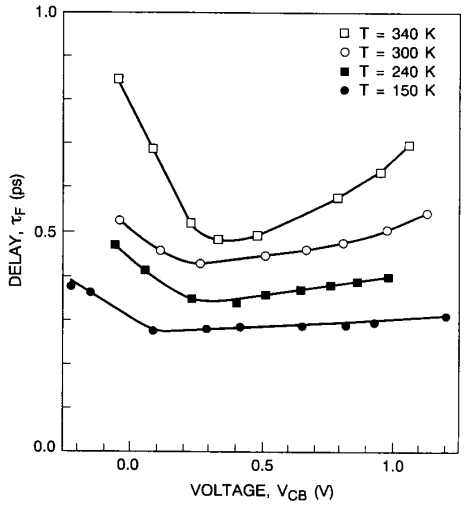

Fig. 10. Small signal forward delay, τ_F, extracted from measured s-parameter measurements for various collector-base biases, V_{CB} and various temperatures, T. The device is an abrupt $InP/_{0.53}Ga_{0.47}As$ n-p-n HBT. 15 mA $\leq I_C \leq$ 20 mA, $A_E = 1.2 \times 10^{-7}$ cm^2, and device layer structure is the same as shown in Table I. The solid line in the figure is to guide the eye.

V. Conclusions

In summary, the microwave performance of abrupt $InP/In_{0.53}Ga_{0.47}As$ n-p-n HBTs has been measured in the temperature range 55 K $\leq T \leq$ 340 K. Our devices have a base thickness $x_B = 500$ Å and a high base doping level $p = 1 \times 10^{20}$ cm^{-3}. The minimum intrinsic small signal emitter-collector forward delay decreases from $\tau_F = 0.5$ ps at $T = 340$ K to a saturated value of $\tau_F \sim 0.28$ ps for $T \leq 150$ K due to a saturation in the inelastic scattering rate. Numerical simulations using the Monte-Carlo technique have been used to model transistor behavior. It is shown that the temperature dependence of electron scattering is responsible for the observed temperture dependence of τ_F. In addition, for $T < 340$ K, the high speed performance of our abrupt $InP/In_{0.53}Ga_{0.47}As$ HBT's may only be explained by the presence of nonequilibrium electron transport in the base and collector.

Acknowledgment

The authors would like to acknowledge M. B. Panish and R. A. Hamm for providing the epitaxial layers. J. Laskar would like to acknowledge the support of M. Feng of the Center for Compound Semiconductor Microelectronics at the University of Illinois, Urbana-Champaign.

References

[1] A. F. J. Levi, B. Jalali, R. N. Nottenburg, and A. Y. Cho, "Vertical scaling in heterojunction bipolar transistors with nonequilibrium electron transport," *Appl. Phys. Lett.*, vol. 60, p. 460, 1991.

[2] R. N. Nottenburg, A. F. J. Levi, B. Jalali, D. Sivco, D. A. Humphrey, and A. Y. Cho, "Nonequilibrium electron transport in heterostructure bipolar transistors probed by magnetic field," *Appl. Phys. Lett.*, vol. 56, p. 2660, 1990.

[3] B. Jalali, Y. K. Chen, R. N. Nottenburg, D. Sivco, D. A. Humphrey, and A. Y. Cho, "Influence of base thickness on collector breakdown in abrupt AlInAs/InGaAs heterostructure bipolar transistors," *IEEE Elec. Dev. Lett.*, vol. EDL-11, p. 400, 1990.

[4] B. Jalali, R. N. Nottenburg, Y. K. Chen, A. F. J. Levi, D. Sivco, A. Y. Cho, D. A. Humphrey, "Near-ideal lateral scaling in abrupt $Al_{0.48}/In_{0.52}As/In_{0.53}Ga_{0.47}As$ heterostructure bipolar transistors prepared by molecular beam epitaxy," *Appl. Phys. Lett.*, vol. 54, p. 2333, 1989.

[5] B. Jalali, R. N. Nottenburg, A. F. J. Levi, R. Hamm, M. B. Panish, D. Sivco, and A. Y. Cho, "Base doping limits in heterostructure bipolar transistors," *Appl. Phys. Lett.*, vol. 56, p. 1460, 1990.

[6] J. Laskar and J. Kolodzey, "Cryogenic vacuum high frequency probe station," *J. Vac. Sci. B*, vol. 8, p. 1161, 1990.

[7] P. J. van Wijnen, H. R. Claessen, and E. A. Wolsheimer, "A new straightforward calibration and correction procedure for on-wafer high frequency s-parameter measurements," *IEEE Bipolar Circuits Technol. Meet. Dig.*, pp. 70-73, 1987.

[8] G. Dambrine, A. Cappy, F. Heliodore, and E. Playez, "A new method for determining the FET small signal equivalent circuit," *IEEE Trans. Microwave Theory Tech.*, vol. 36, p. 1151, 1988.

[9] R. L. Pritchard, *Electrical Characteristics of Transistors*. New York: McGraw-Hill, 1967.

[10] I. E. Getreu, *Modeling the Bipolar Transistor*. Amsterdam, The Netherlands: Elsevier, 1978.

[11] R. J. Trew, U. K. Mishra, W. L. Pribble, and J. F. Jensen, "A parameter extraction technique for heterojunction bipolar transistors," *IEEE Microwave Theory Tech. Dig.*, p. 897, 1989.

[12] G. D. Mallan, *Many Particle Physics*. New York: Plenum, 1986.

[13] P. H. Beton and A. F. J. Levi, "Numerical study of non-equilibrium electron transport in AlGaAs/GaAs heterojunction bipolar transistors," *Appl. Phys. Lett.*, vol. 55, p. 250, 1989.

[14] For a review of the Monte Carlo technique see, for example, C. Jacoboni and L. Reggiani, "The Monte Carlo method for the solution of charge transport in semiconductors with applications to covalent materials," *Rev. Mod. Phys.*, vol. 55, p. 645, 1983; M. V. Fischetti and S. E. Laux, "Monte Carlo analysis of electron transport in small semiconductor devices including band-structure and spacecharge effects," *Phys. Rev.*, vol. B38, p. 9721, 1988; and W. Faucett, A. D. Boardman, and A. D. Swain, "Monte Carlo determination of electron transport properties in Gallium Arsenide," *J. Phys. Chem. Solids*, vol. 31, p. 1963, 1970.

[15] Materials parameters taken from L. W. Massengill, T. H. Glisson, J. R. Hauser and M. A. Littlejohn, "Transient transport in central-valley-dominated ternary III-V alloys," *Solid-State Electron.*, vol. 29, p. 725, 1986.

[16] W. Bardyszewski and D. Yevick, "Influence of temperature on electron transport in bipolar devices," *Appl. Phys. Lett.*, vol. 54, p. 837, 1989.

[17] A. F. J. Levi, "Scaling 'ballistic' heterojunction bipolar transistors," *Electron Lett.*, vol. 24, p. 1273, 1988.

[18] S. E. Laux and W. Lee "Collector signal delay in the presence of velocity overshoot," *IEEE Elect. Device Lett.*, vol. EDL-11, p. 174, 1990.

Joy Laskar (S'84-M'91) received the B.S. degree with highest honors in computer engineering from Clemson University, Clemson, SC, in 1986 and the M.S. degree in electrical engineering from the University of Illinois, Urbana, IL, in 1989 and the Ph.D. degree in electrical engineering from the University of Illinois, in 1991. His Ph.D. research focused on the characteristics of heterostructure transistors at microwave frequencies and cryogenic temperatures.

From 1985 to 1986 he was employed at IBM's Thomas J. Watson Research Center in the advanced sub-micron CMOS group. From Fall 1991 to July 1992 he was a Visiting Assistant Professor with the ECE Department at the University of Illinois and from the Fall of 1992 he has been an Assistant Professor with the EE Department at the University of Hawaii. His research interests include millimeter wave devices and circuits, high-speed device physics and novel device structures.

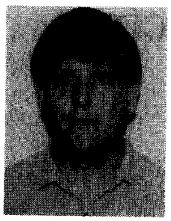

Richard N. Nottenburg (S'79–M'80) was born in Brooklyn, NY. He received the B.S.E.E. degree from Polytechnic Institute of New York, in 1975 and the M.S.E.E. degree from Colorado State University, Fort Collins, in 1978. After receiving his Master's degree he joined the Solar Energy Research Institute as a member of the technical staff. In 1981 he returned to graduate school and received the Ph.D. degree from the Swiss Federal Institute of Technology (EPFL) in Lausanne, Switzerland, in July 1984.

From 1984 to 1991 he worked at AT&T Bell Laboratories and at Bell Communications Research on heterojunction bipolar transistors and circuits. He joined the Faculty of Electrical Engineering at the University of Southern California in 1991, where he is an associate professor. He is engaged in research in high speed electronics and data links for computation systems.

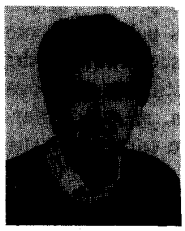

Anthony F. J. Levi was born in London, England. He received the Ph.D. degree from the University of Cambridge, England in 1983.

He joined AT&T Bell Laboratories as a member of technical staff in 1984. In 1993 he joined the University of Southern California as a Professor in the Electrical Engineering Department. His current research interests include nonequilibrium phenomena in transistor and laser devices.

J. A. Baquedano, photograph and biography not available at the time of publication.

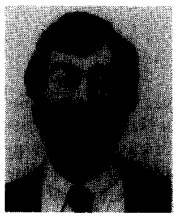

James Kolodzey (S'74–M'74–SM'90) was born in Philadelphia, PA, in 1950. He received the B.S. degree in engineering physics in 1972 and the M.S. in electrical engineering in 1975 from Lehigh University. After working in industry, he returned to graduate school and received the Ph.D. degree in electrical engineering from Princeton University, Princeton, NJ, in 1986 for research on amorphous SiGe alloys.

From 1974 to 1978 he worked at IBM Corporation, and from 1979 to 1982 he worked at Cray Research. He served as Assistant Professor of Electrical Engineering at the University of Illinois at Urbana-Champaign from 1986 to 1990, where he established a laboratory for high frequency device measurements at cryogenic temperatures. In 1987 he was on leave to work on molecular beam epitaxy with A. Y. Cho at AT&T Bell Labs. In 1990 he was on leave to work on SiC and SiGeC alloys with Drs. F. Koch and R. Schwarz at the Technical University of Munich. Since 1991 he has been an Associate Professor of Electrical Engineering at the University of Delaware. His current research interests include the properties of ternary and quaternary alloys of group IV semiconductors, and high-frequency variable temperature characteristics of devices.